Liquefaction Susceptibility of an Earth Dam Foundation: A Case Study

Hatem karoui (hatem.karoui@enit.utm.tn)
National Engineering School of Tunis: Ecole Nationale d'Ingenieurs de Tunis
Mounir Bouassida
National Engineering School of Tunis: Ecole Nationale d'Ingenieurs de Tunis

Research Article

Keywords: Standard Penetration Test (SPT), Earth dam, Liquefaction, Sand, Earthquake, Numerical model

Posted Date: March 15th, 2021

DOI: https://doi.org/10.21203/rs.3.rs-285555/v1

Liquefaction susceptibility of an earth dam foundation: a case study

Abstract:

Sidi El Barrak earth dam is a compacted earth embankment of height 28 m built in 1999 on a heterogeneous foundation with strong dominance of sandy formations. The dam foundation was subjected to several tests to predict its behavior against the liquefaction risk. Standard penetration test (SPT) results served to evaluate the liquefaction risk in an earthquake occurrence.

This article, firstly, presents an interpretation of data collected from SPT tests. Determination of liquefaction risk resulted from the empirical methods proposed by Seed & Idriss, (1985) and Idriss & Boulanger, (2008). Obtained results by those methods showed that, for different earthquake magnitudes equal to 5.25, 6 and 6.75, the risk of liquefaction exists in the pure sand layer located between the ground surface and 15 m depth of the foundation of the earth dam. An UBC3D-PLM constitutive model was adopted for studying the numerical response of sand layer subjected to an earthquake of acceleration equal 0.2 g to estimate its liquefaction risk. Recorded SPT data and laboratory tests results served for the determination of geotechnical parameters of this model. From numerical predictions it revealed that the liquefaction risk is greater for an earthquake characterized by an acceleration equal 0.2 g.

Key Words

Standard Penetration Test (SPT); Earth dam; Liquefaction; Sand; Earthquake, Numerical model;

Main notations

CRR: Cyclic Resistance Ratio

CSR: Cyclic Stress Ratio

CPT: Cone Penetration Resistance

$(N_1)_{60}$: Corrected SPT blows count

M: Earthquake Magnitude

PGA: Peak Ground Acceleration

SPT: Standard Penetration Test

a_{max}: earthquake peak horizontal acceleration (m/s^2)

g: acceleration of gravity (m/s^2)

σ : Total vertical stress (kPa)

σ' : Effective vertical stress (kPa)

F_c: Fines content

1. Introduction:

When an earthquake occurs, the seismic waves propagate from the source up to the ground surface causing a ground shaking. Earthquake effects can be different, such as, structural damages, soil liquefaction and landslides. Soils susceptible to liquefaction risk are mainly loose sands and silts. The liquefaction of saturated loose sands was the cause of numerous damaged buildings, dams and retaining walls for various cases of lived earthquakes, worldwide. Earthquakes of magnitude 8.25 and 6.3 in the USA, caused cracks in the San Andreas earth dam of height 32 m (1906) and the failure of Sheffield earth Dam (1925). In Japan, twelve earth dams composed of sandy soil embankments were damaged in 1939 by an earthquake of magnitude 6.6. The City of Chlef (Algeria) lived severe damages in 1954 and 1980 due to earthquakes of magnitude 6.7 and 7.3, respectively.

For evaluating the liquefaction risk, several empirical methods have been proposed, for instance Seed & Idriss, (1971, 1985), Youd et al., (2001), Cetin at al., (2004) and Idriss & Boulanger, (2008). Those methods involve the comparison between the capacity of the soil against liquefaction resistance expressed in terms of the Cyclic Resistance Ratio (CRR) and the Cyclic Stress Ratio (CSR) caused by the earthquake. Time to time, those empirical methods have been updated by data recorded from SPT and CPT tests related to earthquake case histories. The factors of safety (FS) against liquefaction over the depth of a soil profile were used by Seed et al., (1971 and 1985) to evaluate the liquefaction risk. Soil layers with (FS) greater than 1 are classified non-liquefiable; contrarily when the (FS) is less than one, those layers are considered liquefiable. Further, Iwasaki

et al. (1978) had adopted the factor of safety (FS) to evaluate the liquefaction potential index (LPI). This LPI provides an integration of the factors of safety against liquefaction (FS) over thickness of liquifiable soil layers; then LPI predicts the liquefaction potential causing damage at the ground surface. High level of liquefaction severity corresponds to LPI > 15. In turn, low liquefaction risk level corresponds to LPI < 5. Analysis of a site response investigations subjected to an earthquake solicitation requires in-situ and laboratory to determine the geotechnical parameters of soil layers. Sidi El Barrak earth dam, located near by the City of Tabarka in the North West of Tunisia, (governorate of Jendouba), has a heterogeneous foundation, covering an area of 896 km^2. Storage capacity of the dam equals 265 Million cubic meters of water per year with a normal retaining water height of 27m. Usage of the stored water of Sidi El Barrak earth dam comprises the irrigation of 400 hectares of agriculture lands and electricity production (Karoui & Bouassida, 2016).

This paper aims at highlighting a successful earth dam case study in Tunisia where the vibro-compaction technique, was implemented. Added value was to show the successful design of an earth dam in post construction.

In a recent work, Karoui & Bouassida (2020) analyzed the evaluation of liquefaction risk of the foundation of Sidi El Barrak earth dam using the data recorded from SPTs and by implementing the empirical method proposed by Seed et al., (1985).

In this paper, first, the liquefaction analysis is, in addition studied using the method proposed by Idriss & Boulanger., (2008). Besides the computation of the liquefaction potential index (LPI) using the Luna and Frost, (1998) method is proposed.

Second, a numerical study is implemented by Plaxis 2D software using a soil-column model. Prediction of the liquefaction risk of the dam foundation corresponds is carried out for an earthquake characterized by a horizontal acceleration equals 0.2g. Third, the dynamic analysis, UBC3D-PLM constitutive model proposed by Laera & Brinkgreve (2015) is carried out, for estimating the liquefaction risk of sand formation.

2. Geotechnical and geological investigation of Sidi El Barrak earth dam

2.1 Seismic-tectonic setting of the earth dam site:

The site of Sidi El Barrak earth dam belongs to the African and Eurasian tectonic plate convergence zone of NNO-SSE and NS leadership. The identification of seismic level of this dam has been carried out by a tectonic analysis and historical seismicity with a methodology in accordance with the recommendations of the International Commission of Great Dams. That information allowed adopting an earthquake magnitude of about six and a peak acceleration equal 0.2g. However according to the Tunisian National Institute of Meteorology, the seismic level of the Sidi El Barrak earth dam zone has a magnitude less than 6.

2.2 Geotechnical characterization of the foundation earth dam:

In-situ investigation of the Sidi El Barrak dam foundation included boreholes, pressuremeter tests, SPTs and cored undisturbed samples extracted at different depths. Figure 1 shows the location of main dam location of twelve points of the performed SPTs. The undisturbed samples served for identifying the components and the geotechnical parameters of soil layers from the performed laboratory tests. Those tests, including grain size analysis and Atterberg limits, have been carried out on sand samples extracted by SPT coring device, for determining the fines content and the plasticity index.

Results of those tests permitted to adopt the soil parameters of geotechnical profile of the dam foundation comprising sandy formations up to 50 m depth. The geotechnical profile looks quite heterogeneous and variable both in depth and in plan. Data from a total of hundred and thirteen SPTs permitted to evaluate the liquefaction risk of the dam foundation.

2.2.1 Physical characteristics of sand formations

After results of grain size analysis, sandy soils of Sidi El barrak earth dam foundation is clean, well-graded without fines and characterized by quite uniform grain size distribution. **Figure 2** shows that depth effect is insignificant regarding the shape of all grain size curves of extracted specimens. Table 1 summarizes the physical characteristics of the sand formations crossed in the foundation dam.

2.2.2 Corrections of SPT data

The Standard Penetration Test is an in-situ dynamic test used to estimate the resistance of granular soils, such as, sand and gravel. After several studies carried out, the usage a standard sampling tube during SPT investigation is recommended, for example the "US sampler" with inner diameter equal 35mm (1-3/8). During the SPT investigation carried out on the foundation of Sidi El Barrak dam, the sampler used is "*US sampler" without inner coating of diameter equal 38mm,* which reduces the measured N-value of dense sands about 25-30% and about 10% for loose sands. Sampler is driven into the ground at the bottom of a borehole by blows of sliding "safety hammer" with a mass of 63.5 kg falling over a height equal 76 cm. After seed et al., (1976) the recommended frequency of hammer blows is typically about 30-40 per minute.

Effective stress Correction of N value

Using equation (1), this correction applies to the measured penetration resistance from the SPT (N_m) with respect to an effective overburden stress of 100 kPa:

$$N_1 = N_m \times C_N \tag{1}$$

N_1 is the penetration resistance of the soil subject to an effective overburden stress equals 100 kPa, C_N is a correction factor to determine from the chart given in **Figure 3**.

Correction of drill rods length

Comprehensive studies on the standard penetration test reported when the length of the drill rods is lesser than 10m there is a reflected energy into the rods that reduces the driving energy of the sampling tube into the ground. Hence, the value N_1 determined from Eq (1) is corrected by the multiplying factor **k** applied to the length drill rods. k factor is determined from table 2.

Correction of the type of sampling tube

During the SPT investigation of the foundation of Sidi El Barrak earth dam, the US sampler used of inner diameter, without liner, equals 38mm; leads to N-values lower than those measured by a constant tube diameter of about 10 to 30% for different sand layers. Therefore, a correction applies to increase the measured N-values by the sampling tube without liner by the multiplying correction factor (k') between 10 to 30%. Table 3 shows the values of the correction factor *k'* which depends on the range of N_1 values.

Then, the corrected SPT blows number for effective overburden stress and length of drill rods and the type of sampling tube is:

$$N_2 = N_1 \times k \times k' \tag{2}$$

Further, by introducing the *Energy Rod ratio (ERr)*, it is assumed that 60% of the energy produced by the falling hammer is effectively induced in the SPT sampler, from the corrected (N_2) value given in Eq (2), the novel corrected value $(N_1)_{60}$, is calculated from Eq (3):

$$(N_1)_{60} = N_2 \times \frac{ERr}{60} \tag{3}$$

ERr = energy rod ratio owed to the investigation method,

N_2 is the SPT corrected value.

Investigation carried out for the foundation of Sidi El Barrak dam, used safety hammer with two wraps of a rope around a pulley. Consequently, no correction applies for the studied case, hence the corrected SPT blows count is:

$$(N_1)_{60} = N_2 \tag{4}$$

2.2.3: Interpretation of SPT results

Obtained results from the carried out SPT serve for an empirical determination of the susceptibility to liquefaction of sand formations. Evaluation of the strength parameters of the foundation of Sidi El Barrak earth dam, against seismic acceleration induced by earthquake resulted from 113 tests

carried out between 1 to 52 m depth. Those tests were performed within twelve boreholes (**Figure 1**).

After results from the SPTs and the geological profile of the foundation of Sidi El Barrak earth dam, two different zones are distinguished in the river bed and in the left bank have different resistance parameters.

- Zone of river bed

In this zone, seven SPT borings (SPT1, SPT2, SPT3, SPT4, SPT9, SPT10 and SPT11) including 47 tests, were executed between 1 and 30.5m depth. Recorded values of SPT, $(N_1)_{60}$ led to the consideration of two formations: crossed sand layers from the ground surface up to 15 m depth, then crossed sand layers beyond 15m depth.

$(N_1)_{60}$ values of the upper sand formation located at less than 15m depth are in the range 6 to 24; adopted average value is $(N_1)_{60}$ = 14.

The values of $(N_1)_{60}$ of the lower sand formation, located beyond 15m depth, range between 20 and 34; the adopted averaged value is $(N_1)_{60}$ = 29.

- Zone of the left bank:

In this zone 66 tests were executed within borings (SPT5, SPT6, SPT7, SPT8 and SPT12) between 1m and 51m depth. The interpretation of SPT results values of $(N_1)_{60}$ allowed distinguishing between two sandy formations: sands located at depth less than 7m, and sand formation between 7m and 51 m depth. Results of $(N_1)_{60}$ allowed distinguishing a first set of values where $2 \leq (N_1)_{60} \leq 8$, with adopted averaged value $(N_1)_{60}$ = 4.6. The second set comprises values $(N_1)_{60}$ in the range of 12 to 26 with the averaged value $(N_1)_{60}$ = 19.

Second set $(N_1)_{60}$ values fit with values recorded in the sandy formation located beyond 7m depth.

The values of $(N_1)_{60}$ of the sand layers located at depth greater than 7m are comprised between 9 and 32. The averaged value for the sandy formation is $(N_1)_{60}$ = 20. Further, measurements showed

$(N_1)_{60}$ values greater than 36, as obtained at relatively high depths (from 24 to 51m). The existence of pebbles formations and cemented sands may explain those relatively high $(N_1)_{60}$ values.

3. Methods for estimation liquefaction risk

Among numerous contributions, Seed & Idriss (1985), then Idriss & Boulanger (2008) proposed empirical methods to evaluate the liquefaction risk induced by earthquakes. Based on the cyclic stress ratio induced by the earthquake, the estimation of the soil capacity to resist against liquefaction. Further, the evaluation it comes of a factor of safety calculated from the Cyclic Resistance Ratio (CRR) and the Cyclic Stress Ratio (CSR). Using the peak horizontal acceleration at ground surface equals to 0.2g and the SPT results, one can estimate the cyclic resistance of the foundation of Sidi El Barrak dam against an earthquake. It is noted that sands layers having $(N_1)_{60}$ greater than 30 are considered non liquefiable.

3.1 Cyclic stress ratio (CSR)

The cyclic stress ratio (CSR), at a given depth in a soil deposit can be determined from equation (5):

$$CSR = 0.65 \times \left(\frac{\sigma_v}{\sigma'_v} \right) \left(\frac{a_{\max}}{g} \right) \times r_d \qquad (5)$$

$a_{\max}$ is the peak horizontal acceleration of earthquake at ground surface, g is the acceleration of gravity, σ_v and σ'_v denote the total and effective initial vertical stresses, respectively.

r_d is the shear stress reduction factor that accounts for the dynamic response of the soil profile; this factor is given by Eq (6):

$$r_d = \begin{cases} 1.0 - 0.00765 \times z & z \le 9.15m \\ 1.174 - 0.0267 \times z & 9.15m \ \pi \ z \le 23m \\ 0.7444 - 0.008 \times z & 23m \ \pi \ z \le 30m \\ 0.5 & z \ \phi \ 30m \end{cases} \qquad (6)$$

z is the depth counted from the ground surface, in meters.

3.2 Cyclic resistance ratio (CRR)

According to several methods, in-situ tests data serve for determining the cyclic resistance ratio (CRR). The normalized penetration resistance $(N_1)_{60}$ as introduced for the correction of SPT data. As for results obtained from the Cone Penetration Test (CPT), one adopts the values of normalized cone penetration resistance (q_{c1N}), as explained for the SPT case.

Two methods by Seed and Idriss (1985) and Idriss and Boulanger (2008) for determining the CRR are briefly presented in the following.

Seed and Idriss (1985) method:

Cyclic resistance ratio (CRR) is determined from the corrected SPT blows count $(N_1)_{60cs}$. After Seed et al. (1985), there followed by Blake (2001), the corrected SPT blows count is calculated from equation (7):

$$\left(N_1\right)_{60cs} = \alpha + \left[\beta \times \left(N_1\right)_{60}\right] \tag{7}$$

Coefficients α and β in equation (7) depend on the percentage of fines content (F_c) of sand. For clean sands: $F_c \leq 5\%$ $\alpha = 0$ and $\beta = 1$, for $F_c > 35\%$ $\alpha = 5$ and $\beta = 1.2$. In case $5 < F_c \leq 35\%$ α and β are determined from equations (8) and (9), respectively.

$$\alpha = \exp\left[1.76 - \left(\frac{190}{F_c^{\,2}}\right)\right] \tag{8}$$

$$\beta = \left[0.99 + \left(\frac{F_c^{\,1.5}}{1000}\right)\right] \tag{9}$$

Then, the CRR value for an earthquake of magnitude M = 7.5 is calculated from equation (10) by using the method proposed by Youd et al. (2001);

$$CRR_{M=7.5} = \frac{1}{34-(N_1)_{60cs}} + \frac{(N_1)_{60cs}}{135} + \frac{50}{\left[10\times(N_1)_{60cs}+45\right]^2} - \frac{1}{200} \tag{10}$$

For a different magnitude, i.e. M ≠ 7.5, after equation (11) the corrected CRR is:

$$CRR = CRR_{7.5} \times M_{sf} \tag{11}$$

M_{sf} is a correction factor which applies for an earthquake of magnitude different from 7.5, M_{sf} is determined from equation (12)

$$M_{sf} = \left(\frac{M}{7.5}\right)^{-2.56} \tag{12}$$

Idriss and Boulanger (2008) method:

Idriss and Boulanger, (2008) introduced the Cyclic Resistance Ratio (CRR) for estimating the soil resistance against liquefaction from SPT data. Equation (13) enables the calculation of the CRR for an earthquake of standard magnitude M = 7.5.

$$CRR_{M=7.5} = \exp\left[\frac{(N_1)_{60cs}}{14.1} + \left(\frac{(N_1)_{60cs}}{126}\right)^2 - \left(\frac{(N_1)_{60cs}}{23.6}\right)^3 + \left(\frac{(N_1)_{60cs}}{25.4}\right)^4 - 2.8\right] \tag{13}$$

In equation (13), the corrected blows count $(N_1)_{60cs}$ is calculated from equation (14).

$$(N_1)_{60cs} = (N_1)_{60} + \exp\left(1.63 + \frac{9.7}{F_C + 0.01} - \left(\frac{15.7}{F_C + 0.01}\right)^2\right) \tag{14}$$

For an earthquake of magnitude M ≠ 7.5, and the effective overburden stress is different from 100 kPa, Idriss & Boulanger (2008) recommended to correct the calculated CRR from equation (13) by using the multiplying factors M_{sf} and K_σ.

K_σ = correction factor of overburden stress as determined from equation (15).

$$k_\sigma = 1 - C_\sigma \ln\left(\frac{\sigma'_v}{P_a}\right) \leq 1 \quad (15)$$

P_a = the atmospheric pressure;

Coefficient C_σ depends on in situ measurements of $(N_1)_{60}$; it can be determined in terms of the $(N_1)_{60cs}$ by using equation (16).

$$C_\sigma = \frac{1}{18.9 - 2.55\sqrt{(N_1)_{60cs}}} \leq 0.3 \quad (16)$$

3.3 Liquefaction risk analysis

The approach by Seed et al (1985) suggested the critical penetration resistance N_{crit}. When $N_{crit} \geq (N_1)_{60cs}$, the liquefaction potential becomes critical. *In the zone of Bed River, the water table level coincides with the ground surface. In turn, the water table level is located at 5m depth from the ground surface in the left bank zone.*

Further, for sand formations located in the bed of river, the critical penetration resistance calculated for different earthquake magnitudes vary between 11 and 20.4. Comparing those estimations with corrected blows count, one note that the liquefaction potential is greater for sands located at depth less 15m. In turn, sand formations located at depth beyond 15m are not susceptible to liquefaction (**Figure 4**).

However, for sands located in the left bank, the value of critical penetration resistance, calculated at different magnitudes and depths, is in the range 5.5 to 10. Comparison of those predictions with estimated corrected blows count shows that for the upper sand formation (depth less than 7m), the averaged value of N_{crit} is greater than $(N_1)_{60cs}$ values comprised between 2 and 8. Therefore, the liquefaction risk is significant in the upper sand formation (depth lesser than 7m) (**Figure 5**). Underneath the upper sand layer (depth beyond 7m), the averaged value of critical penetration

resistance remains lower than the corrected blows counts value. Therefore, this sand formation is non-liquefiable when subject to for earthquakes of magnitude M ≤ 6.75.

Figures 6 and 7 present the estimated CSR and CRR of the sand layers, of the foundation of Sidi El Barrak dam, located in the left bank zone at depth 0 - 7m and in the bed river zone at depth 0 - 15m, respectively. The Cyclic Stress ratio (CSR) is estimated for different values of the earthquake magnitude (M) versus the reference curve of CRR proposed by Idriss & Boulanger (2008). For the two sand formations, the increase in magnitude (M) leads to an increase of the Cyclic Stress Ratio (CSR); hence, the liquefaction risk becomes more significant. From **figures 6 and 7**, one can note that $(N_1)_{60cs} > 22$ for sand layers in the bed river (figure 6), and $(N_1)_{60cs} > 12$ for sand layers in the left bank zone (figure 7), this confirms that sand formations of foundation of Sidi El barrak dam are classified non liquefiable. For an earthquake of magnitude M = 7.5, 78% of recorded data are located above the reference curve (**Figure 6)**, whilst, only 20% of recorded data are located above the reference curve for an earthquake magnitude M = 5.25. Such result highlights that the liquefaction risk is more susceptible for an earthquake characterized by magnitude M > 5.25 for sand layers located at depth of 15m and 7m in the bed of river and in the left side of the foundation of Sidi El Barrak earth dam, respectively. Further, for an earthquake of magnitude M < 5, the risk of liquefaction remains insignificant.

3.4 Evaluation of liquefaction potential index (LPI)

The liquefaction potential index (LPI) quantifies the severity of liquefaction and predicts its area of propagation of liquefaction and related damage. In other words, the LPI characterizes the failure potential of a liquefaction-prone area (Luna and Frost, 1998).

The calculation of LPI by using SPT results consists in integrating the factor of safety (FS) over a soil column up to 20m depth, at given specific location.

The factor of safety against liquefaction, traducing the liquefaction potential, is the ratio between the CRR and the CSR, as defined by equation (17).

$$FS = \frac{CRR}{CSR} \tag{17}$$

Iwasaki et al. (1978, 1982) proposed the calculation of the liquefaction potential index (LPI) from equation (18):

$$LPI = \int_0^{20} F(z).w(z)dz \tag{18}$$

z = depth at mid thickness of the soil layer (0 to 20 m); dz = the depth differential increment. The weighing factor, w(z), and the severity factor, F(z), are calculated using Eqs (19-22):

$$F(z) = 1 - FS \text{ for } FS < 1 \tag{19}$$

$$F(z) = 0 \text{ for } FS \geq 1 \tag{20}$$

$$w(z) = 10 - 0.5z \text{ for } z < 20m \tag{21}$$

$$w(z) = 0 \text{ for } z \geq 20 \tag{22}$$

For a soil column of thickness lower than 20m, Luna and Frost, 1998 suggested the calculation of LPI from equations (23) and (24).

$$LPI = \sum_{i=1}^{n} w_i.F_i.H_i \tag{23}$$

$$F_i = 1 - FS_i \text{ for } FS_i < 1 \tag{24}$$

$$F_i = 0 \text{ for } FS_i \geq 1 \tag{25}$$

n is the number of soil layers.

FS_i = the factor of safety for i-th layer; the weighing factor is w_i =10–0.5 z_i;

z_i is the depth at midst thikness of i-th layer (m); H_i is thickness of the discretized soil layers; F_i = liquefaction severity of i-th layer.

The classification of the level of liquefaction severity with respect to LPI has been carried out following the recommendations proposed by Iwasaki et al. (1982), Luna and Frost (1998), and MERM (2003), as summarized in **Table 4**.

The liquefaction potential index (LPI) has been determined by using (SPT data) at depth less than 20m of the soil profiles (SPT4 in the river bed zone and SPT7 in the left bank zone) of the foundation of Sidi El Barrak earth dam subject to an earthquake of magnitude equals 5.25, 6 and 6.75 and a peak ground acceleration equals 0.2g.

Tables 5, 6 and 7 present the computed LPI in the riverbed zone for earthquake magnitudes M =5,25, M= 6 and M = 6,75. The LPI of the sand column is very high when the magnitude is M > 6.

For a sand column located in the left bank (SPT7), Tables 8 and 9 show that computed liquefaction potential index increase when the magnitude is M > 6.

Estimation of the LPI is in agreement with the above obtained results that showed the liquefaction risk is greater for the sand layers located at depth lower than 15m in the riverbed zone, and at depth lower than 7m in the left bank zone of the foundation of Sidi El Barrak dam.

4. Liquefaction risk: numerical investigation

4.1 Modeling and boundary conditions

Numerical simulation of the liquefaction risk of sand formations of the foundation of the Sidi El Barrak earth dam was carried out by the finite element (FE) code Plaxis 2D. Adopted plane strain model boundary conditions are an infinite horizontal surface of depth extending up to 50m. A soil-column model **(Figure 8**) of 40m height, 2.5m width, has been built to investigate the propagation of seismic waves using SPT7 data located in the left bank. Following the recommendation by Laera and Brinkgreve (2015), the horizontal dimension of this model fits with the required element length.

Based on SPT recorded values (N_{SPT}) the geotechnical profile of soil-column column comprises five sand layers with water table located at 5.35m depth from the ground surface level. The liquefaction risk, of those five sand layers, is studied by using the UBC3D-PLM model (Makra, 2013). Several updates of the UBC3D-PLM model for liquefaction analysis are available: for instance, Tsegaye, (2010) and Petalas & Gavali, (2013).

The generated mesh by Plaxis 2D software (V9.2D) comprises 15 nodes triangular finite elements. The computation process of liquefaction risk by Plaxis code comprises static and dynamic stages. In the static stage, default fixities were applied, i.e normally fixed vertical boundaries' and a fully fixed base. In the dynamic stage, the vertical boundaries are modeled with tied degrees of freedom and a prescribed displacement at the bottom boundary (figure 8). The dynamic calculation has been carried under an earthquake characterized by a peak horizontal acceleration equals to 0.2g and of magnitude M = 6.5.

4.2 Geotechnical parameters of UBC3D-PLM model

The UBC3D-PLM model is used for evaluating the liquefaction risk of a soil column subjected to propagated seismic wave with an undrained dynamic computation. The liquefaction risk in the sandy soil is expressed by means of the excess pore pressure ratio (r_u) given by Eq (26).

$$r_u = 1 - \frac{\sigma_v^{'}}{\sigma_{v0}^{'}} \tag{26}$$

$\sigma_v^{'}$ = the vertical effective stress at the end of dynamic calculation and $\sigma_{v0}^{'}$ is the initial effective vertical stress.

When the value of r_u is greater than 0.7 the sandy soil is considered liquefiable, Beaty and Perlea (2011).

The geotechnical parameters of the model depend on the value of corrected blow count $(N_1)_{60}$. Beaty & Beyrne (2011) and Makra (2013) proposed five correlations given by Equations (27, 28, 29, 30 and 31) to calibrate the model based on SPT results as follows:

$$\phi_P = \phi_{CV} + \frac{(N_1)_{60}}{10} + \max\left(0; \frac{(N_1)_{60} - 15}{5}\right) \quad (27)$$

$$K_G^e = 21.7 \times 20 \times (N_1)_{60}^{0.3333} \quad (28)$$

$$K_B^e = 0.7 \times K_G^e \quad (29)$$

$$K_G^P = K_G^e \times (N_1)_{60}^2 \times 0.003 + 100 \quad (30)$$

$$R_f = 1.1 \times (N_1)_{60}^{-0.15} \quad (31)$$

ϕ_P = the peak friction angle of sand, ϕ_{CV} = the friction angle at constant volume, K_G^e = the elastic shear modulus, K_G^P = the plastic shear modulus and K_B^e = the elastic bulk modulus, R_f = the failure ratio.

Table 10 summarizes the adopted parameters of UBC3D-PLM model considered for evaluating the liquefaction risk of the foundation of Sidi El Barrak earth dam.

4.3 Results and discussions

Figure 9 shows the deformed mesh at the end of the dynamic analysis of liquefaction risk. From this figure, the deformation is mostly concentrated between the ground surface and 15m depth, i.e. in the upper sand layers of the sand column model. In this upper sand layer, the corrected blow count is $(N_1)_{60}$ = **6.5** which refers to a weak resistance when consider an earthquake with a peak acceleration equals 0.20g. The predicted deformation of soil column justifies the previous observations which indicated that the significant liquefaction risk is predicted in the upper sand layer located between the ground surface and 15m depth of the foundation of Sidi El Barrak earth dam.

Figure 10.a shows that maximum values of excess pore pressure are predicted in those upper sand layers. Consequently, the effective stresses in those upper sandy layers is almost zero (**Figure 10.b**). Besides, the liquefaction risk is ascertained in terms of the excess pore pressure ratio (r_u) which values are shown in **Figure 11**. It is noted that r_u values are greater than 0.7 in the upper sand layers. In turn, those values are lesser than 0.7 in the sand layers beyond 15m depth. After r_u values the upper sand layers located before 15m depth are vulnerable to liquefaction caused by an earthquake of peak ground acceleration equals 0.2g.

Figure 12, displays the produced maximum horizontal displacement in the foundation by an earthquake with a peak acceleration equal 0.2g. Maximum horizontal displacement equal 8cm corresponds to the maximum equivalent static force that caused the same maximum deformation induced by an earthquake after 10 s of the dynamic time.

The maximum amplitude of the peak ground acceleration at depth 7m from the ground surface is equal to 0.3 g (**Figure 13**). The signal has been filtered by the sand layer, since its peak acceleration has increased from -0.2 g to -0.3 g is induced by the dynamic forces subjected to the soil column model.

From the above comparative analysis between estimation by empirical methods and numerical predictions, it is concluded that the susceptibility against liquefaction risk is prominent in the upper loose sand formation.

5. Conclusion

This paper studied the analysis of the risk of liquefaction of sand formations of the foundation of Sidi El Barrak earth dam.

First, the geotechnical characterization of the foundation with focus on the interpretation of recorded SPT data was addressed.

Empirical methods proposed by Seed & Idriss (1985) and Idriss & Boulanger (2008), were implemented, then, related estimations of the liquefaction potential risk, were compared.

Numerical predictions of the behaviour of dam foundation were obtained from a dynamic analysis performed by the Plaxis finite element Code, to evaluate the liquefaction risk in sand layers of the foundation of Sidi El Barrak dam. Also, their dynamic behavior has been studied when subjected to earthquakes with peak acceleration equals 0.2 for three magnitudes (5.25, 6 and 6.75). For all magnitudes, it was proven that the liquefaction risk is much more significant for the sand layers located at depth less than 15m in the river bed. The most susceptible sand layers to liquefaction are located between the ground surface and 7m depth. The second approach consisted of a dynamic analysis using the finite element code Plaxis 2D. The UBC3D-PLM model has been adopted for five sand layers which parameters were derived from the SPT data and laboratory test results. Predictions by Plaxis code, were found in good agreement with results found by using the two empirical methods, i.e., Seed and Idriss, (1985) and Idriss & Boulanger, (2008).

References:

Beaty, M.H. and Byrne, P.M. (2011). UBC sand constitutive model. Itasca UDM website 904aR.

Beaty, M.H. and Perlea, V.G. (2011). Several observations on advanced analyses with liquefiable materials. Thirty first annual USSD conferences on 21st century dam design-advances and adaptations, 1369-1397

Ben Salem, Z., Frikha, W., and Bouassida, M. (2017). Effects of densification and stiffening on Liquefaction Risk of Reinforced Soil by Stone Columns. J. Geotechnical. Geoenvironmental Eng., ASCE

BRGM/EDF (1991) Résultats des essais statiques de laboratoire. Rapport d'expertise globale. Juin 1991: Annexe 1, A13, France.

BRGM/EDF (1991) Résultats des essais statiques de laboratoire. Rapport d'expertise globale. Juin 1991: Annexe 14 A44, France.

BRGM/EDF (1991) Résultats des essais statiques de laboratoire. Rapport d'expertise globale. Juin 1991: Annexe 45 A82, France.

Cubrinovski, M. and Ishihara, K. (2002). "Empirical correlation between SPT N value and relative density for sandy soils". Soils and foundations, Vol 39, No. 5, pp. 61–71.

De Alba, P., Seed, H.B. and Chan, C.K. (1999). "Sand liquefaction in large scale simple shear tests", Journal of Geotechnical Engineering Division, ASCE, Vol. 102, No. GT9, Paper 12403, Sept., 1976, pp. 909-927.

El Ouni, M.R., Bouassida, M and Das, M.B. (2009). Vibrocompaction improvement of Tunisian liquefiable sands. Proc. 17th ICSMGE'09. M Hamza et al (Eds.) 5th – 9th October, Alexandria (Egypt). IOS Press, Vol 3, 2366-2369.

Idriss, I.M and Boulanger, R.W., (2008). "Soil liquefaction during Earthquakes". Oakland, California, USA. : Earthquake Engineering Research Institute.

Iwasaki, T., Tokida, K., Tatsuoka, F., and Yasuda, S. (1978). A practical method for assessing soil liquefaction potential based on case studies at various sites in Japan, Proceedings of 2nd International Conference on Microzonation, San Francisco, 885–896.

Iwasaki, T., Tokida, K., Tatsuoka, F., Watanabe, S., Yasuda, S., and Sato, H. (1982). Microzonation for soil liquefaction potential using simplified methods, Proceedings of 2nd International Conference on Microzonation, Seattle, 1319–1330.

Johari, A. and Khodaparas, A.R. (2013). "Modelling of probability liquefaction based on standard penetration tests using the jointly distributed random variables method". Engineering Geology, 158, 1-14.

Karoui, H. and Bouassida, M., (2020). Assessment of liquefaction risk by Standard Penetration Test (SPT): Foundation of Sidi El Barrak Dam (Tunisia). 4th International Conference on Geotechnical Engineering (ICGE20). 09-11 March 2020.

Karoui, H. and Bouassida, M., (2016). Assessment of observed of behavior of Sidi El Barrak Dam (Tunisia). Innov. Infrastruct. Solut. (2016) 1:44, 1-9.

Laera, A.and Brinkgreve, R.B.J., (2015). Site response analysis and liquefaction evaluation. Delft University of Technology & Plaxis BV, The Netherlands.

Luna, R. and Frost, J. D. (1998). Spatial liquefaction analysis system, J. Comput. Civil Eng., 12, 48–56.

Makra, A. (2013). Evaluation of the UBC3D-PLM constitutive model for prediction of earthquake induced liquefaction on embankment dams. Msc Graduation Thesis, Delft University of Technology, Plaxis, (pp. 1-112).

Microzonation for Earthquake Risk Mitigation (MERM) (2003). Microzonation Manual,World Institute for Disaster Risk Management.

Petalas, A. and Galavi, V. (2013). Plaxis liquefaction model UBC3D-PLM model. Plaxis knowledge base.

Roberston, P.K. and Wride, C.E (1997). "Cyclic liquefaction and its evaluation based on SPT and CPT. In NCEER Workshop.

Seed, H.B., Tokimatsu, K., Harder, L.F. Jr and Chung, R (1985). «Influence of SPT procedures in soil liquefaction resistance evaluations". J. Geotech. Engrg., ASCE111 (12), (pp. 1425–1445).

Tsegaye, A. (2010). Plaxis liquefaction model. External report. Plaxis knowledge base.

Youd, T.L., Idriss, I.M., Andrus, R.D., Castro, G., et al (2001). «Liquefaction resistance of soils: summary report from the 1996 NCEER and 1998 NCEER/NSF workshops on evaluation of liquefaction resistance soils". J. Geotechnical and Geoenvironmental Eng., ASCE 127 (10), (pp. 33–817).

List of figures

List of Tables

Figures

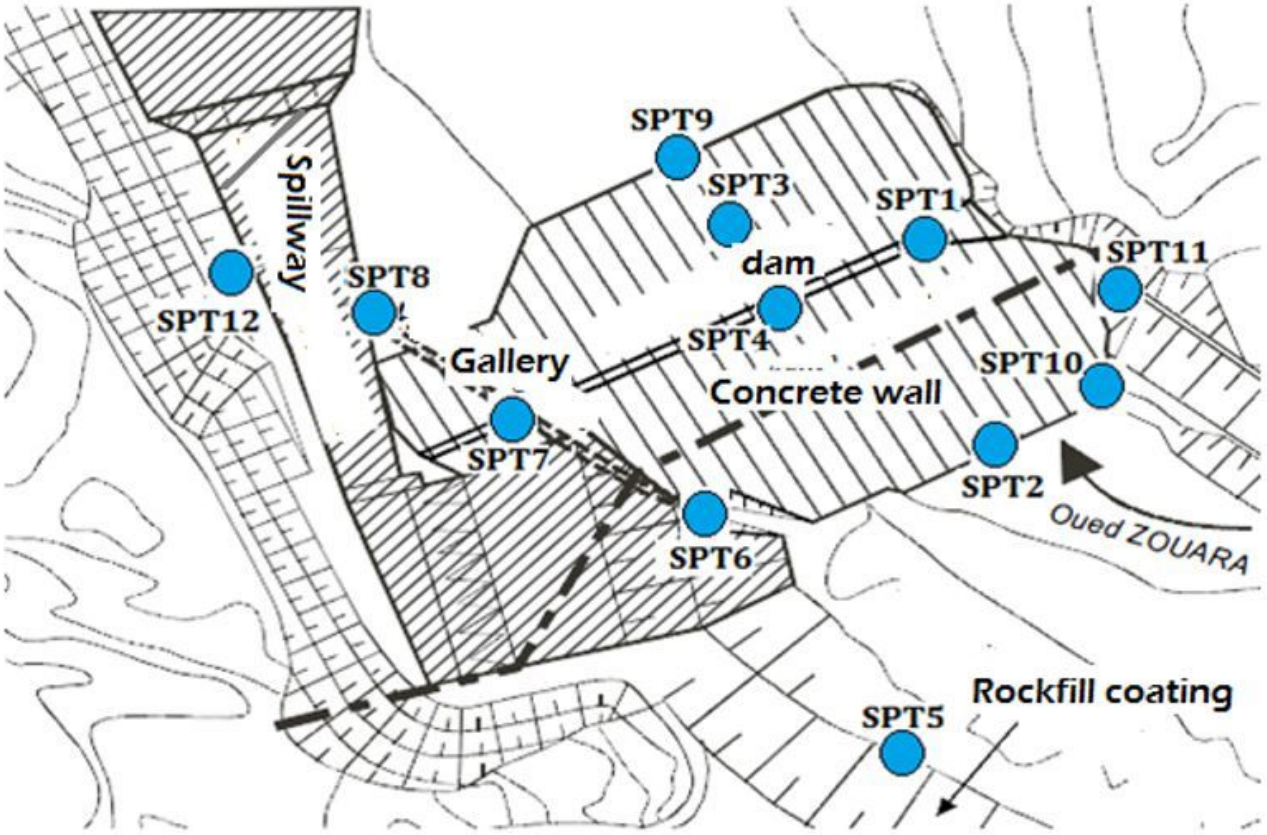

Figure 1

Locations of SPT executed on the foundation of Sidi El Barrak dam

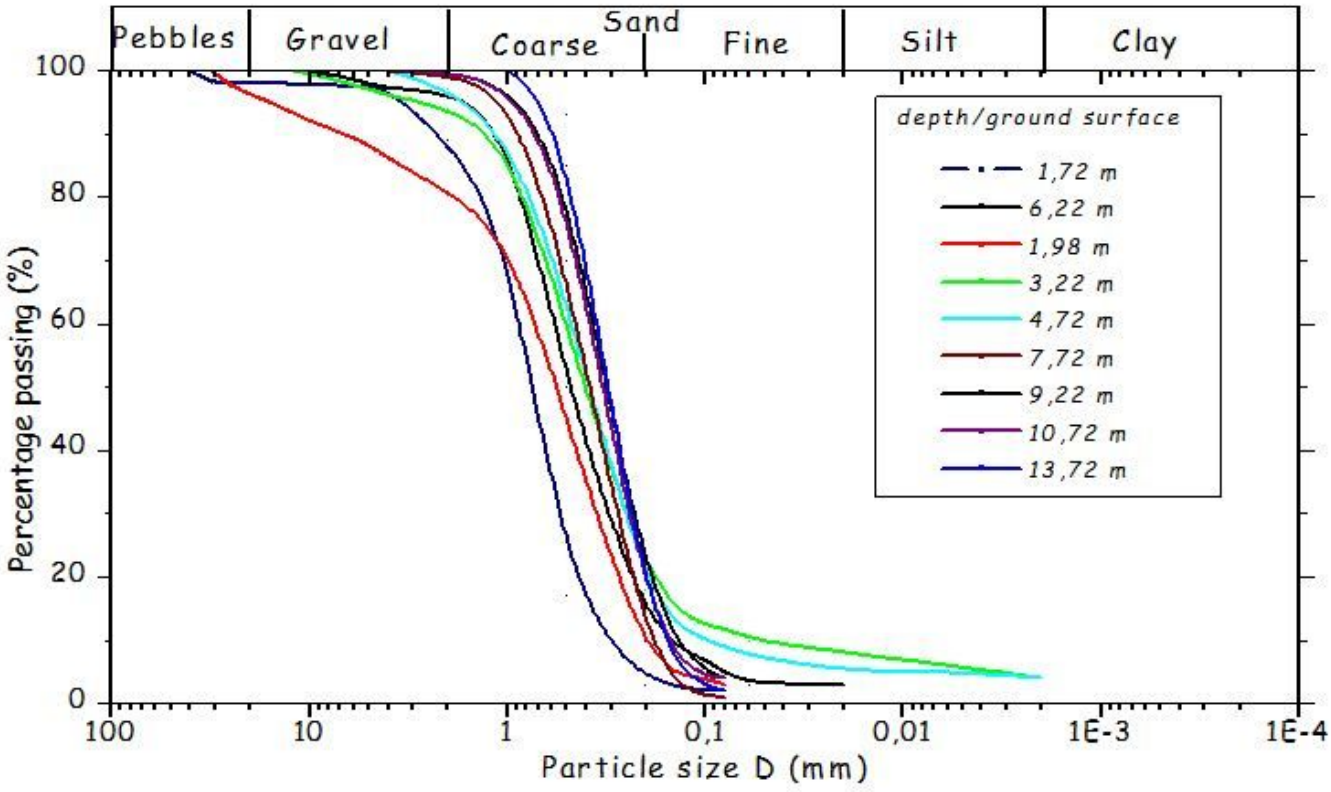

Figure 2

Grains size distributions of upper sand formation

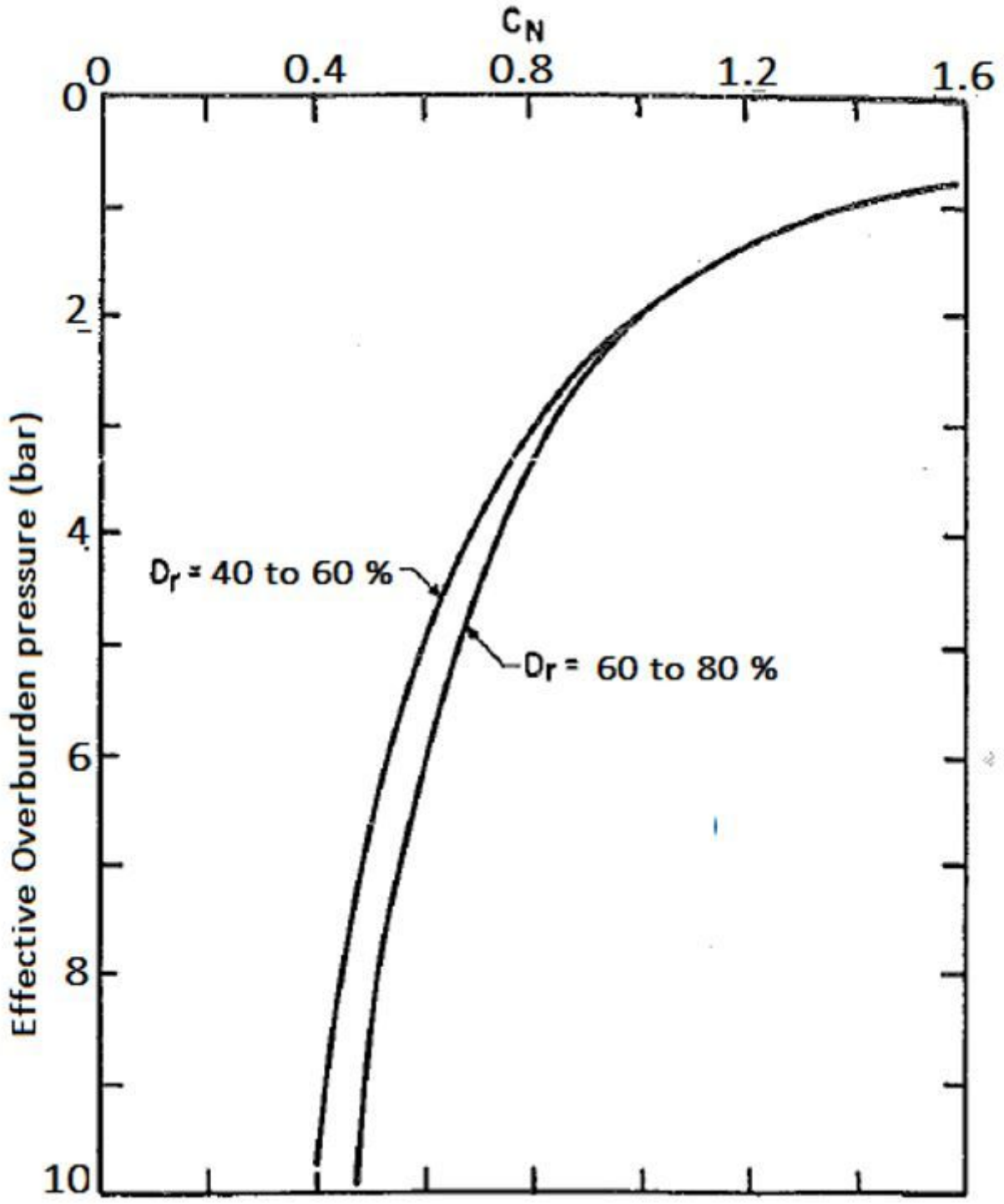

Figure 3

Chart for determination of CN values

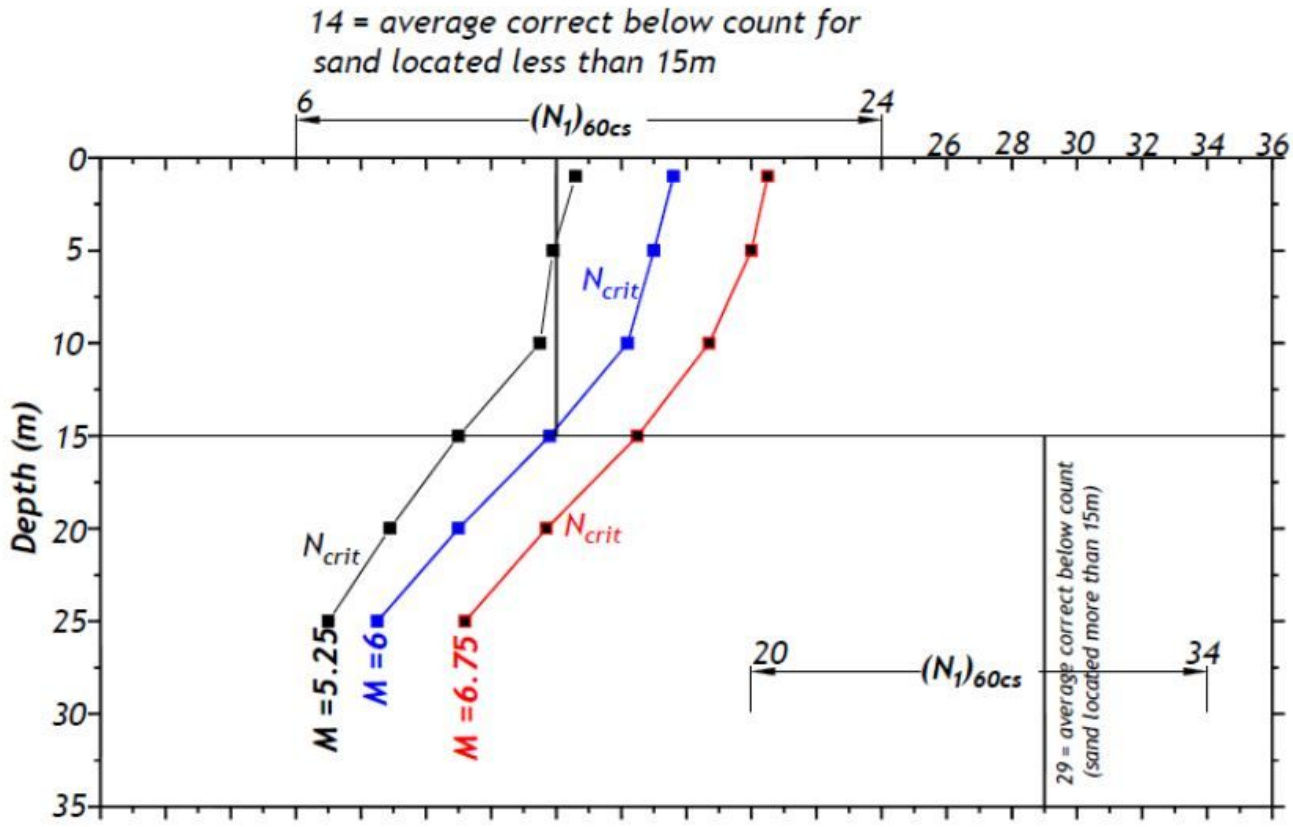

Figure 4

Comparison between (N1)60cs and Ncrit area of the bed river zone

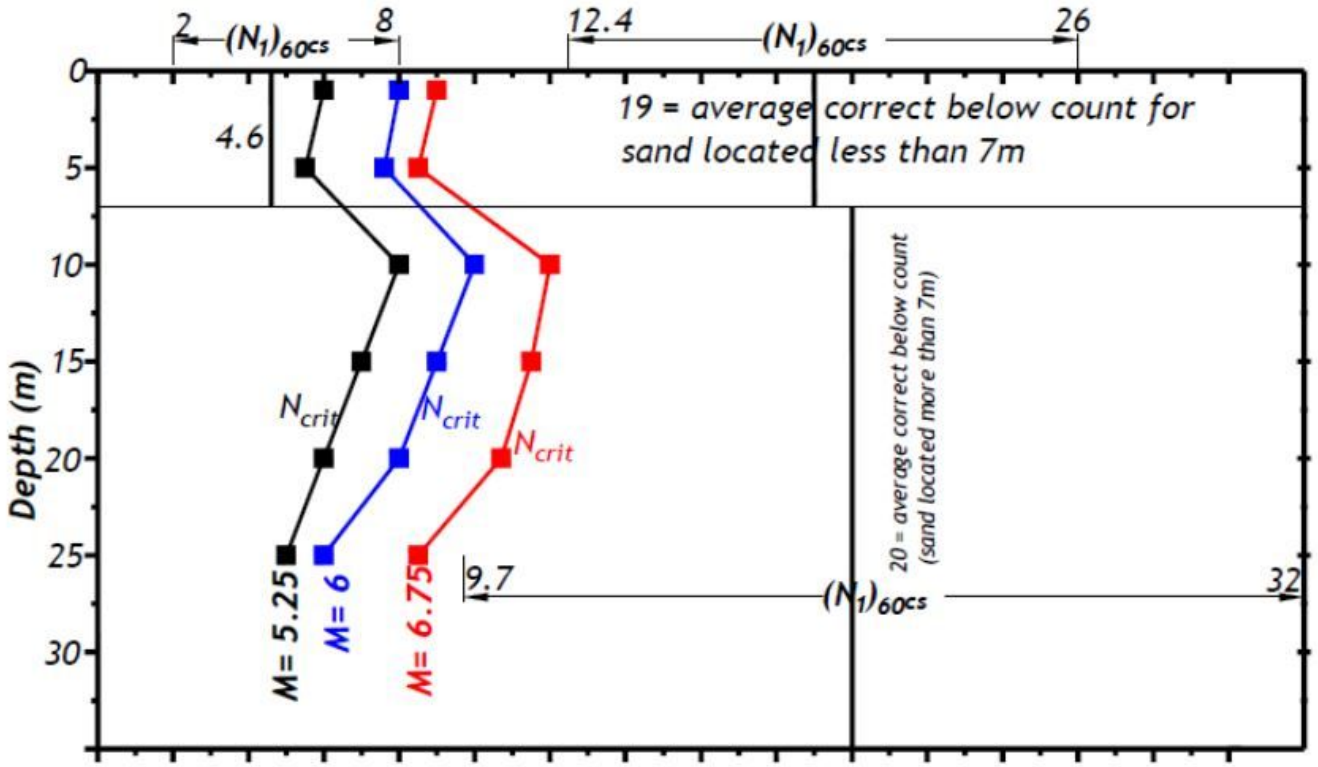

Figure 5

Comparison between (N1)60cs and Ncrit , left bank zone

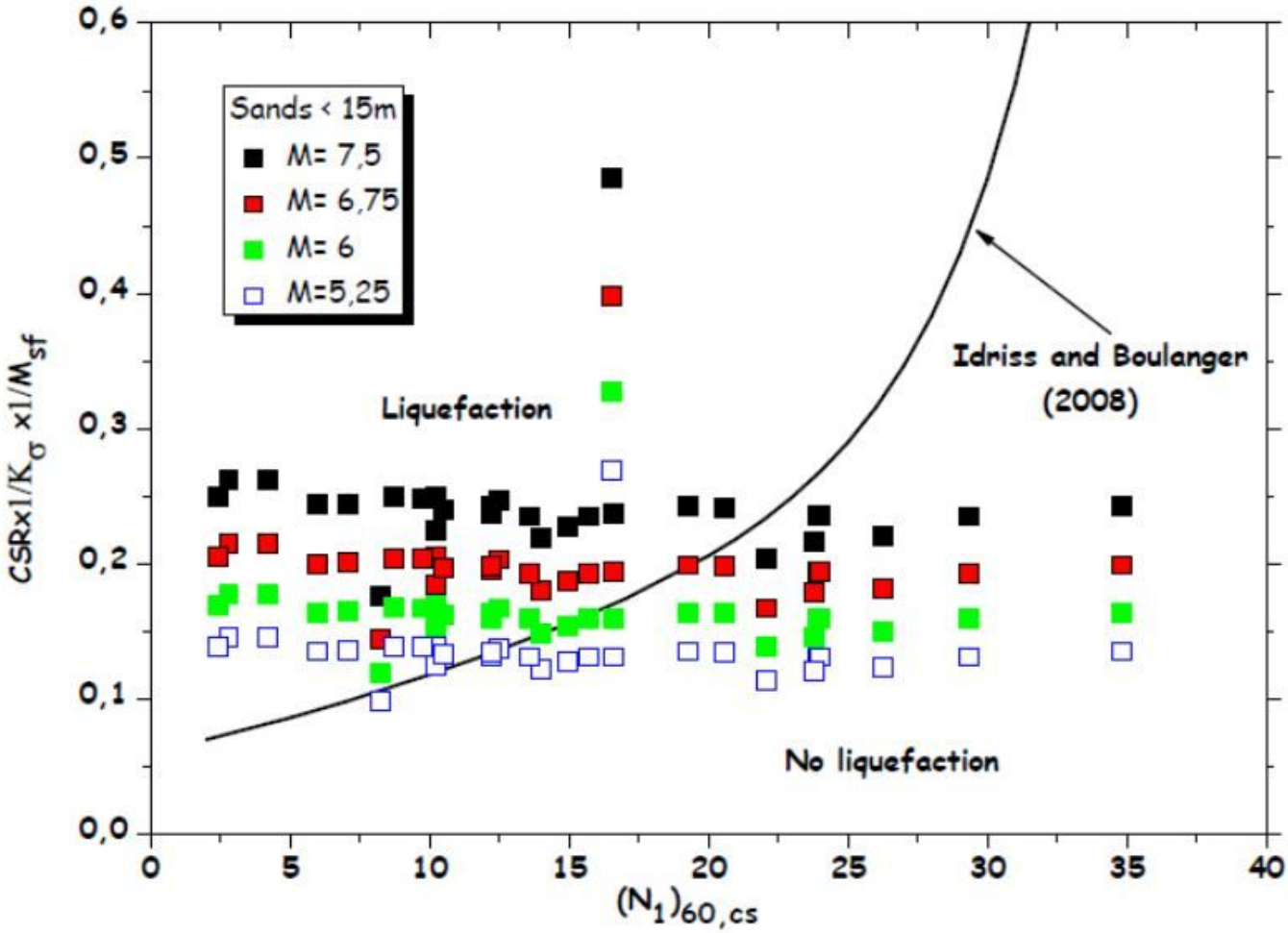

Figure 6

Relationship between cyclic stress ratio (CSR) and (N1)60cs

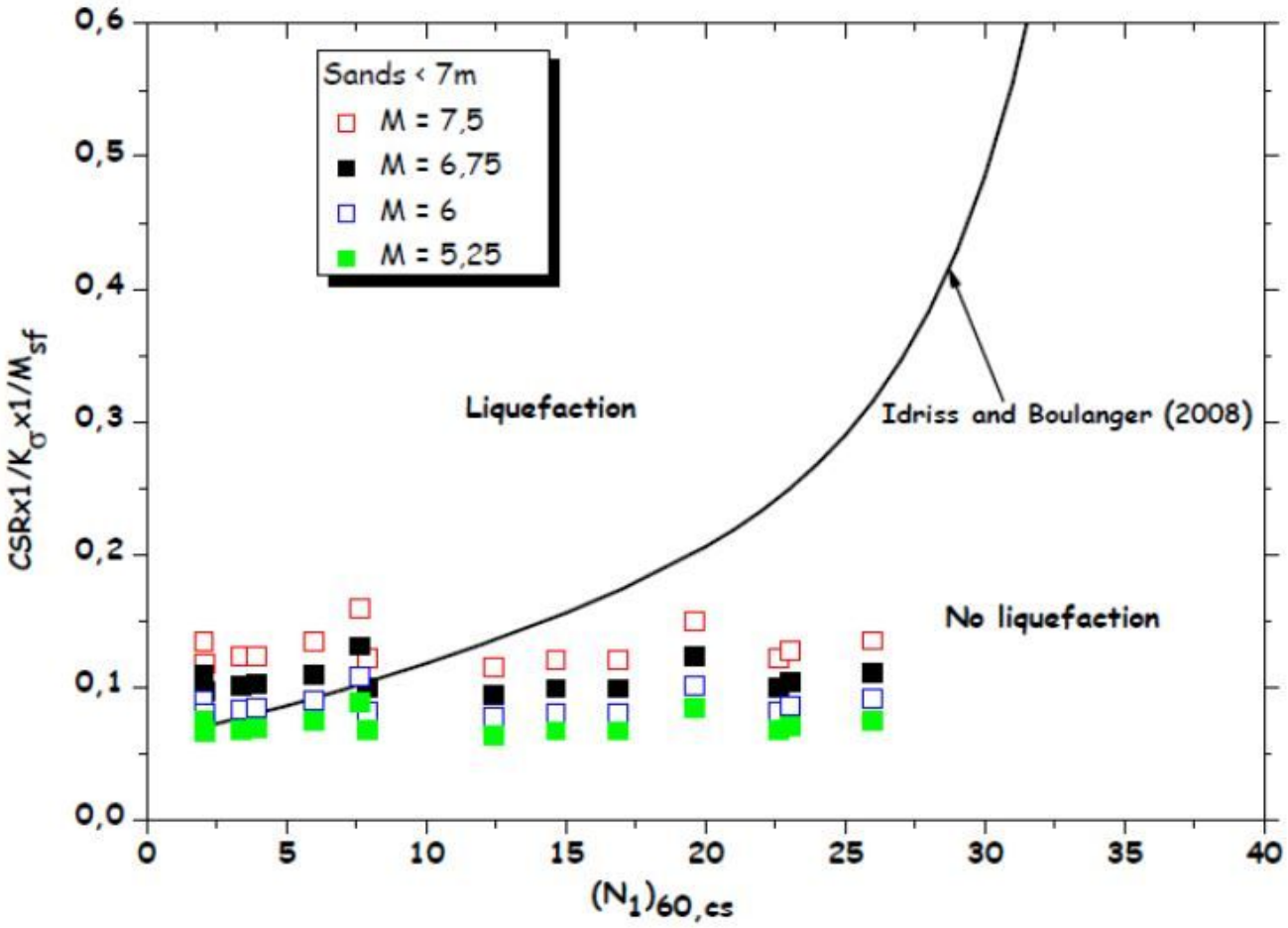

Figure 7

Relationship between cyclic stress ratio (CSR) and (N1)60cs

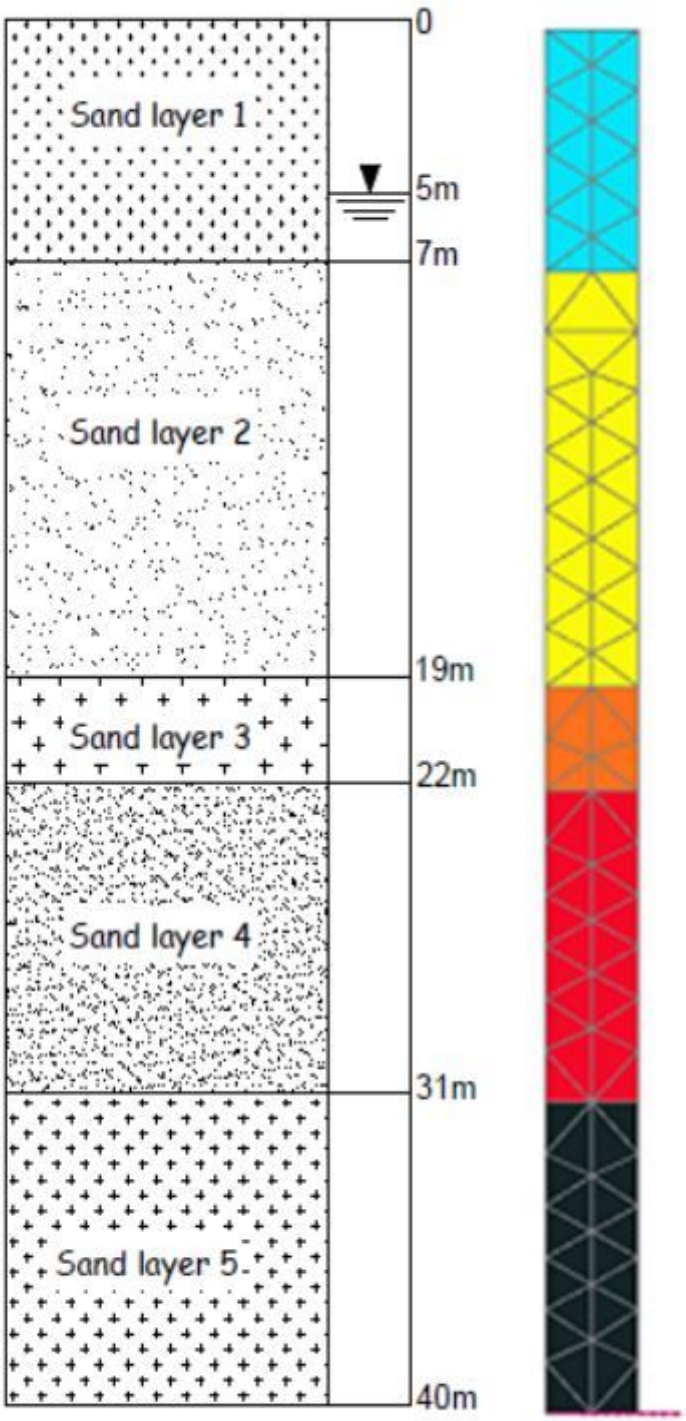

Figure 8

Mesh and boundary conditions of numerical soil-column model

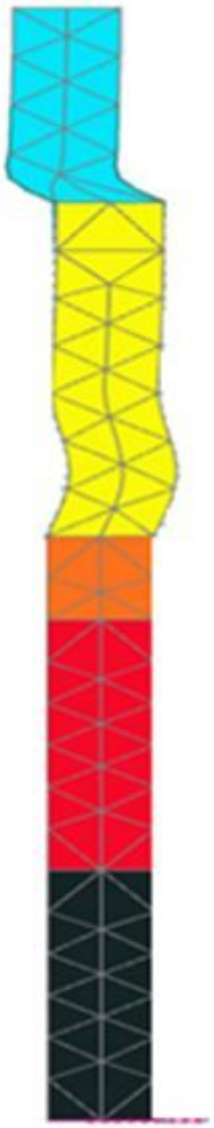

Figure 9

Deformed mesh at the end of the dynamic analysis.

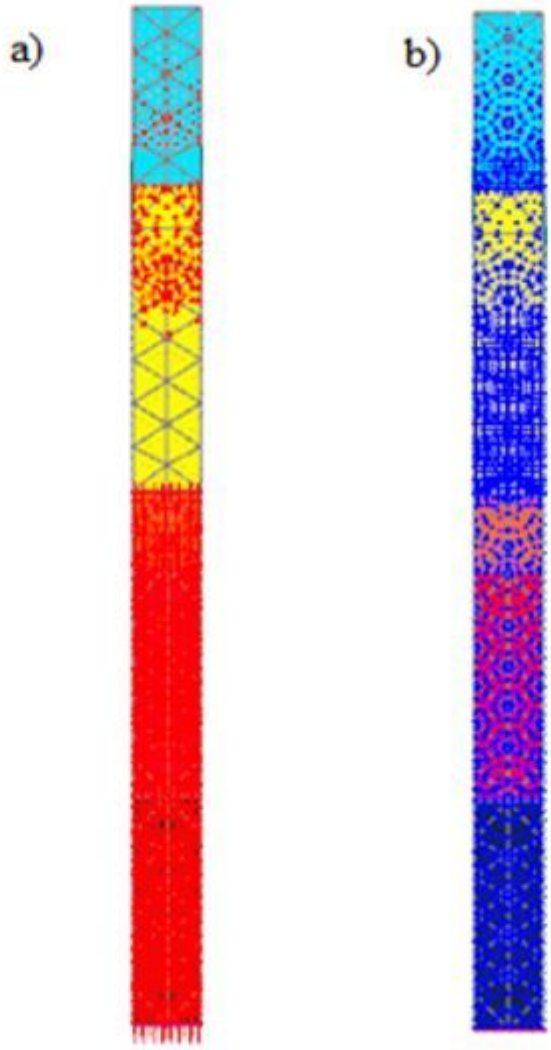

Figure 10

Effective stresses (a) and Excesses pore pressure (b)

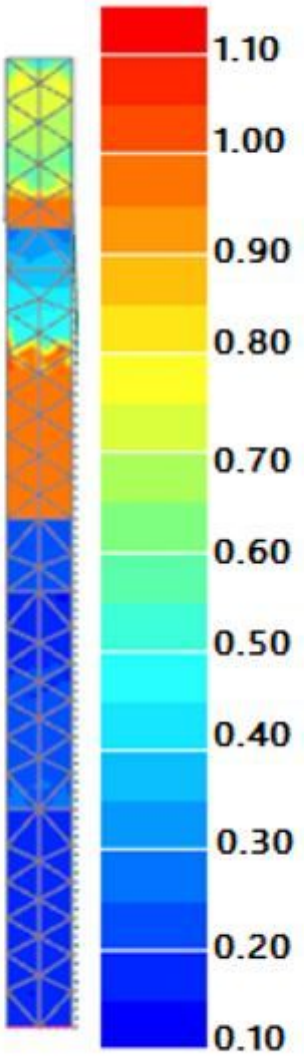

Figure 11

Pore pressure ratio (ru) distribution

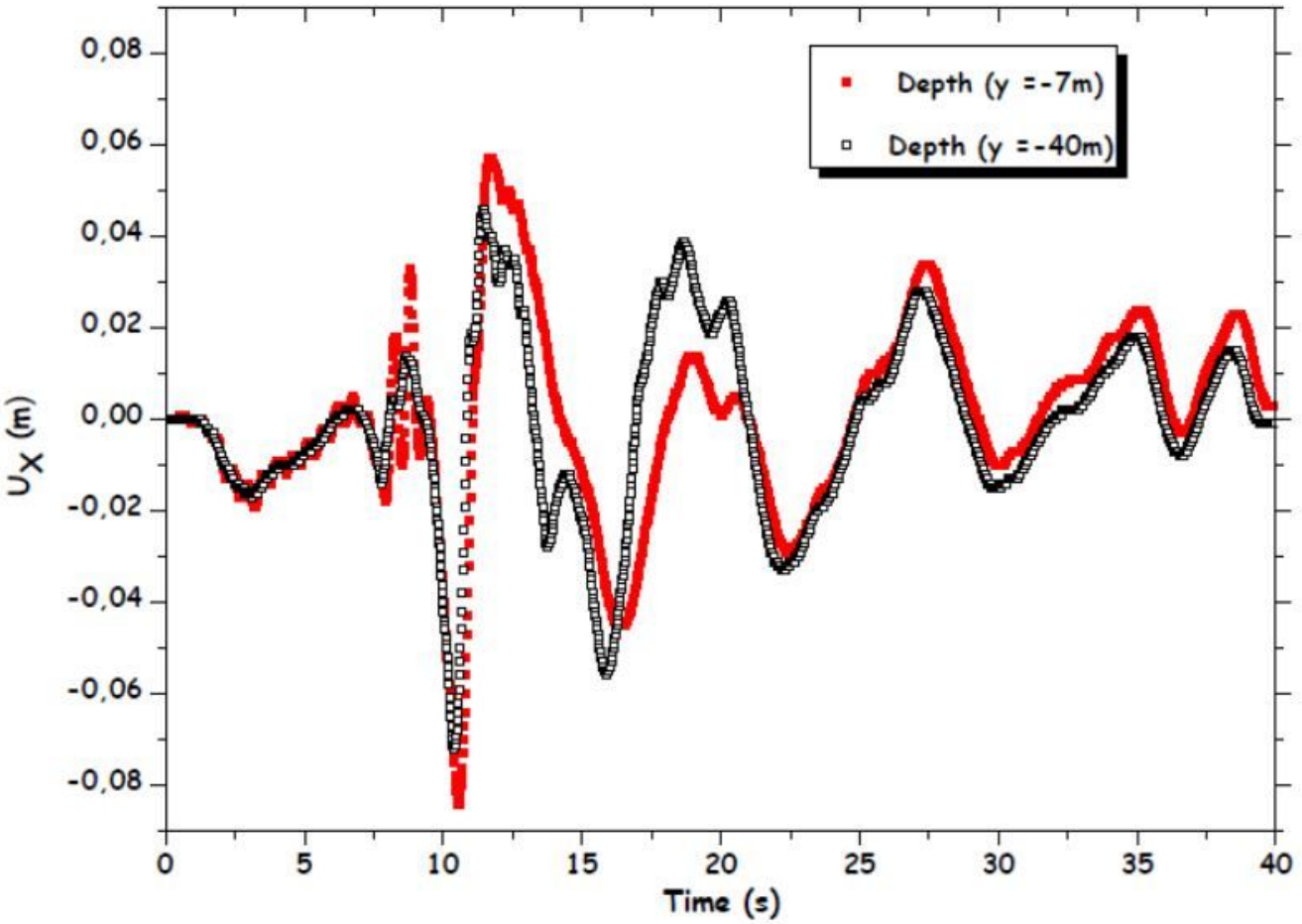

Figure 12

Evolution of the horizontal displacement at depth between (-7m) and (-40m) from the top level

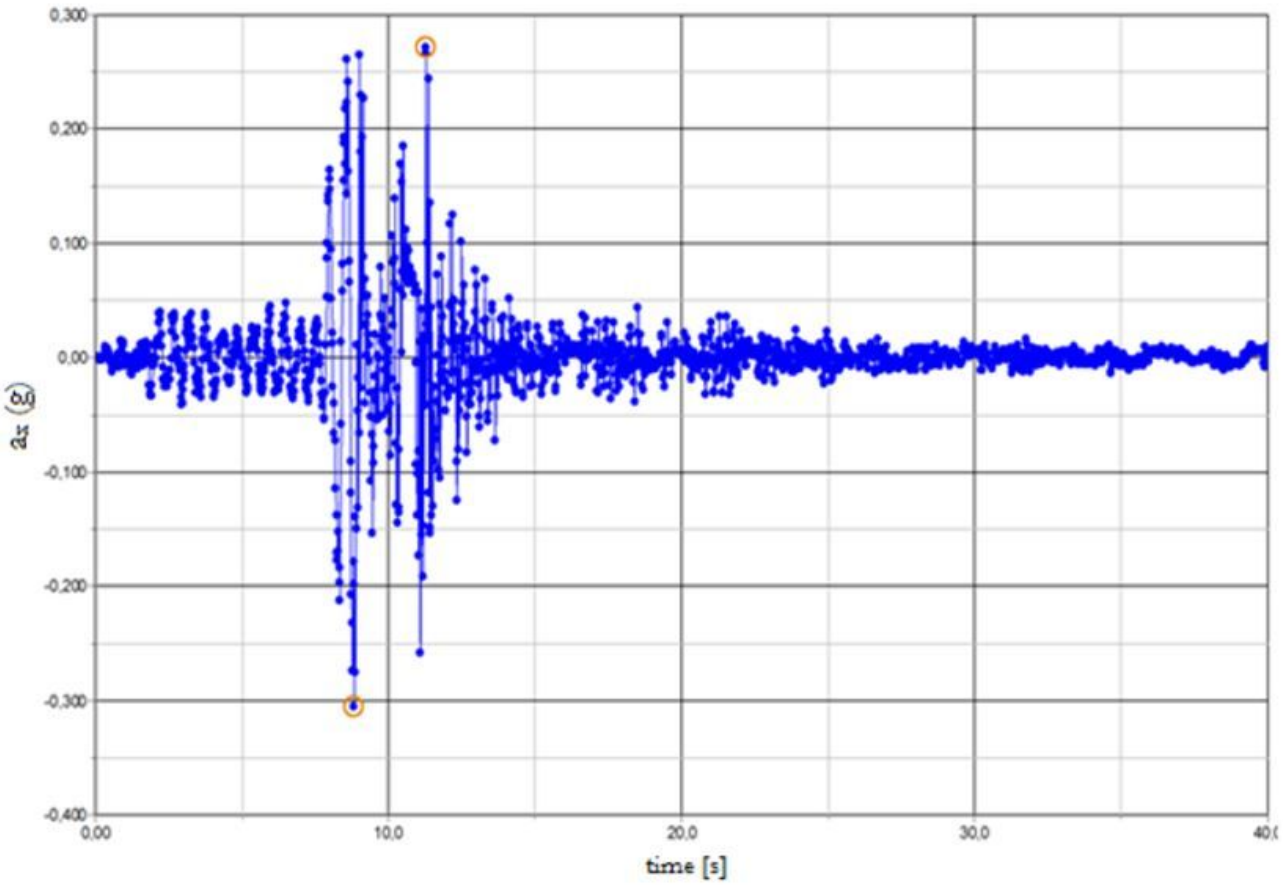

Figure 13

Accelerogramme (ax) at -7m depth from the surface level

Supplementary Files

This is a list of supplementary files associated with this preprint. Click to download.

- Tables1n10.docx